Development of High-Throughput and High-Content Analysis Assays for Neurodegeneration-Related Intrinsically Disorderd Proteins

Noah Nathan

Laboratory of Molecular Therapeutics

Department of Biomedical Engineering

University of Minnesota

Spring 2020

Introduction

Intrinsically disordered proteins (IDPs) are proteins that lack a three-dimensional ordered structure, property which is encoded in its sequence. These proteins exist in what is called an ensemble of conformations that allow for multiple intramolecular or intermolecular interactions with other structured proteins or IDPs [1]. Another result of their intrinsic disorder is that under certain conditions, IDPs can misfold and aggregate into oligomer and fibril structures which have been associated with neurodegenerative diseases [2].

One of such proteins is Fused in Sarcoma (FUS), a 526 amino-acid RNA binding protein that contains a prion-like, nuclear localization and nuclear export sequence. FUS normally localizes to the nucleus, but is actively transported to the cytoplasm upon various cellular stress insults [3]. In the nucleus, FUS is involved in DNA damage repair and splicing. When FUS is trafficked to the cytoplasm, it plays a role in mRNA stabilization and transport, as well as stress granule assembly. These granules are dynamic; however, it is believed that chronic stresses can slow down their kinetics and act as seeds for protein aggregation. Cytoplasmic FUS aggregates have been observed in Amyotrophic Lateral Sclerosis (ALS) and Frontotemporal Lobar Degeneration (FTLD). Moreover, FUS mutations are associated with 4% of familial forms of ALS as well as sporadic cases of this disease [4]. Mislocalization and aggregation of wild-type or mutant FUS and its association with neurodegeneration pathology makes this protein a potential therapeutic target [4].

A second IDP of interest is alpha-synuclein, which can form insoluble fibril structures present in the brains of Parkinson's disease, Alzheimer's disease and other alpha-synucleinopathy patients. Alpha-synuclein is mostly expressed in the brain and localizes to the synaptic terminals, where it is thought to interact with the lipid bilayer and regulate synaptic vesicle exocytosis [5]. Recently, alpha-synuclein has been shown to colocalize with damaged DNA sites, suggesting it also plays a role in double stran break repair [6]. Due to its important roles in the human CNS, preventing the aggregation and formation of toxic species of alpha-synuclein is also a potential therapeutic target.

IDPs associated to neurodegenerative diseases, such as FUS and alpha-synuclein, represent a major challenge in terms of the development of drugs that can rescue their toxicity. Since no static structure of these proteins really exists, rational design of drugs that target oligomers is a difficult task [1]. In order to overcome this, the Laboratory of Molecular Therapeutics has focused its efforts on conducting FRET-based high-throughput screens (HTS) for small molecule drugs that can modulate protein-protein interactions and key cellular processes such as autophagy and the proteasomal pathway. To assess the hits obtained from HTS FRET experiments, we propose using high-content image analysis (HCA) to probe for cellular processes relevant to each neurodegenerative disease being studied.

In this project, we sought to develop HTS and HCS assays relevant to FUS and alpha-synuclein. For FUS, we developed a time-resolved FRET biosensor that allows for HTS of compounds that can modulate stress granule and irreversible aggregate formation. In addition, we developed a MATLAB script capable of segmenting stress granules and aggregates from fluorescence microscopy images of FUS-expressing cells. For alpha-synuclein, we focused our efforts on developing a MATLAB script capable of segmenting neurite outgrowth from brightfield images of neurospheres.

This project is relevant as it provides a robust and multifaceted platform for drug discovery in the neurodegeneration space. Moreover, the screening platform and computational tools developed here can be applied to any protein involved in liquid-liquid phase separation (LLPS) and neurite outgrowth.

Methods

Cell Culture

HEK-293 (human embryonic kidney) and N2a (neuroblastoma) cells were cultured in phenol red free DMEM (Gibco) supplemented with 10% FBS (Gibco), 5 mL Penicillin/Streptomycin (HyClone) and 5 mL GlutaMax (Gibco) at 37 °C and 5% CO2. SH-SY5Y (neuroblastoma) cells were maintained in the same culture conditions, except for F-12 DMEM (Corning).

Neurosphere Culture

SH-SY5Y cells were passaged at 80% confluency and plated into 10 cm petri dishes for transfection. Lipofectamine 2000 reagent was used to transfect cells with 10 ug DNA of either N-terminal tagged GFP-wildtype aSyn plasmid or N-terminal tagged GFP-A53T aSyn plasmids. 48 hours after transfection, SH-SY5Y cells were passaged and resuspended in differentiation medium #1 (DMEM F-12, 10% FBS, % P/S and 10 µM retinoic acid) for 5 days. The resuspended SHSY5Y were plated into 6 well plates at a density of 100,000 cells/well and rotated at 80 rpm on a platform rotator at 37˚C and 5% CO_2. After 5 days, the media was changed to differentiation medium #2 (DMEM F-12 and 5 ng/mL brain derived neurotropic factor (BDNF)). After 5-7 days, the neurospheres were plated on laminin-coated glass bottom plates in differentiation medium #2. After 24 hours of attachment, neurites began to grow out of the neurospheres. Three days after attachment the neurospheres were imaged.

Förster Resonance Energy Transfer (FRET) Measurements

For transfections, HEK-293 cells were plated at 70% confluency in six 10 cm dishes (2x donor only, 2x donor/acceptor, 2x control). HEK-293 cells were transfected with either 7.5 ug of FUS-GFP (1:0, donor only) or 0.8 ug FUS-GFP/6.7 ug FUS-RFP (1:8, donor/acceptor) using Lipofectamine 3000. Cells were incubated for 48 hours at 37˚C and 5% CO_2. At that point, one donor only, one donor/acceptor and one control plates were treated with 24 uL of MG-132 for 1 hour. In preparation for Fluorescence Lifetime measurements, cells were lifted using TrypLE (Gibco) for 5 minutes. The cells were then pelleted, washed 3 times using 10 mL of PBS (Corning), and resuspended at 1,000,000 cells/mL. Cells were dispensed into 384-well plates and FRET was measured using a Fluorescence Lifetime plate reader (FLT-PR), using the GFP-RFP settings as described in the instrument's manual. FRET efficiency was calculated through the fluorescent lifetime of the donor molecule (GFP) by itself and in presence of the acceptor (RFP), as shown in Equation 1. Fluorescent lifetime data was filtered so that all data points had an intensity within 90 and 150 mV, which ensures a proper FLT measurement.

$$E = 1 - \frac{\tau_{DA}}{\tau_D} \quad \text{Equation 1}$$

Stress Granule Induction

N2a cells were plated at 100,000 cells/well in a 6-well plate. After 24 hours, cells were transfected with 1 ug FUS-GFP using Lipofectamine 3000. After 24 hours, each condition was treated with 0.4 M sorbitol and 5 uL MG-132. After an hour of treatment, each well was fixed with 1 mL of 4% paraformaldehyde for 20 minutes at room temperature, followed by washing with PBS and Hoechst staining. Cells were image using an Evos FL microscope.

Site-Directed Mutagenesis

Mutagenesis of FUS-GFP and FUS-RFP constructs was performed via QuikChange mutagenesis with custom primers ordered to create the disease-associated R495X (truncation) and P525L (point) mutations. PCR reactions consisted of 1 uL PfuUltra DNA polymerase, 5 uL 10x reaction buffer, 1 uL dNTP mix, 50 ng of FUS plasmid, 1 uL of 10 uM Forward+Reverse primer mix, 1.5 uL DMSO (3%) and NF-H_2O up to 50 uL. After the PCR reaction, samples were digested with DpnI and transformed into XL1-Blue competent bacteria. Colonies were picked after 24 hours, and mini-preps were sent to ACGT for DNA sequencing. Sequence alignments were performed in ApE (A plasmid Editor) software.

Image Processing

Stress Granule Counting Algorithm

Stress granules were isolated from GFP channel images by several image processing operations, such as cropping, opening, intensity thresholding and watershed transforming. Different thresholds were tested to assess the robustness and inherent bias of the algorithm. Nuclear regions were isolated using the same pipeline; however, gray thresholding was used for all DAPI channels. Total stress granules were obtained by counting the objects in the GFP channel. Nuclear aggregates were found by multiplying the logical matrices of DAPI and GFP channels. Finally, cytoplasmic granules were obtained by subtracting the two previous values.

Automated Neurite Outgrowth Quantification Algorithm

Total neurite length was extracted from brightfield microscopy images of neurospheres at 20x. Background was removed via an opening operation with a disk morphological structural element. Next, images were thresholded, closed and filtered for objects smaller then 50 pixels. The resulting logical matrices were then processed with a linear morpholohical structural element, which was convoluted with the image at angles 0-360 to obtain neurites in all directions. Finally, total neurite length was summed and normalized to the arclength of the neurosphere, which was measured using ImageJ.

Manual ImageJ Neurite Outgrowth Quantification

Starting from the same images used in the automated analysis, neurites were tracked manually using the Simple Neurite Tracer plugin in ImageJ. Total neurite length was summed and normalized to the arclength of the neurosphere.

Results

High-Throughput Time-Resolved FRET Measurements of FUS-FUS Interactions

Förster resonance energy transfer (FRET) measurements allow for exquisite spatiotemporal resolution of protein interactions in live cells. FRET is based on the phenomena of energy transfer between fluorophores, which is proportional to the inverse sixth power of distance (FRET ~ $1/d^6$) between the donor (GFP) and acceptor (RFP) molecule. This energy transfer can cause a decrease in donor fluorescent lifetime, which is a measure of the average time needed for a fluorophore to transition from the excitation to the emission state. Previous projects on FUS focused on engineering the FRET biosensor in terms of total plasmid DNA and donor to acceptor ratio. The next step in developing this biosensor was to collect enough fluorescent lifetime data points of FUS-GFP and FUS-RFP in order to obtain the standard deviation of the system. In future drug screens, the standard deviation will be used as a reference to identify hits. We further tested the response of the biosensor to the proteasome inhibitor MG-132, which has been shown to induce stress granule formation [7]. As shown in Figure 1, the donor only (FUS-GFP) fluorescent lifetime on both conditions was that of 2.65 ns, which has been reported in other studies [8]. In addition, the lifetime of donor/acceptor samples was significantly lower; however, MG-132 treatment did not induce further reduction in FLT. Based on the untreated condition data, we determined a standard deviation of 0.0158 ns. In future drug screens the threshold for hits will be set at 2.45 ± 0.0474 ns (3 SD).

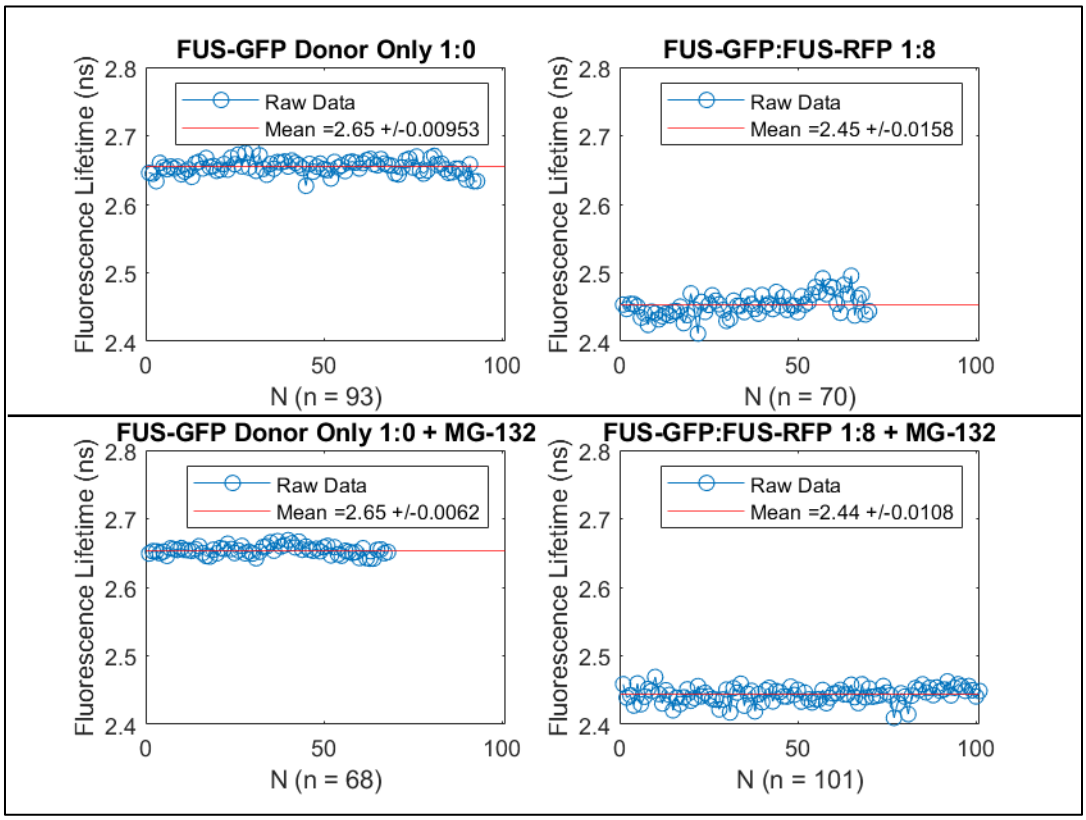

Figure 1. Raw FUS biosensor fluorescent lifetime data. Top: Untreated WT FUS biosensor fluorescence lifetime reads. Bottom: MG-132 treated WT FUS biosensor lifetime reads.

The fluorescent lifetime data points shown in Figure 1 were averaged across the number of samples for each condition and FRET was calculated. As shown in Figure 2, the FRET efficiencies obtained were that of 7.61% for the untreated biosensor and 7.93% for the MG-132 condition. Statistical analysis showed that the donor only lifetime was significantly higher than the donor/acceptor lifetime of each condition. Furthermore, we found that the untreated donor/acceptor was also significantly higher than the MG-132 donor/acceptor condition.

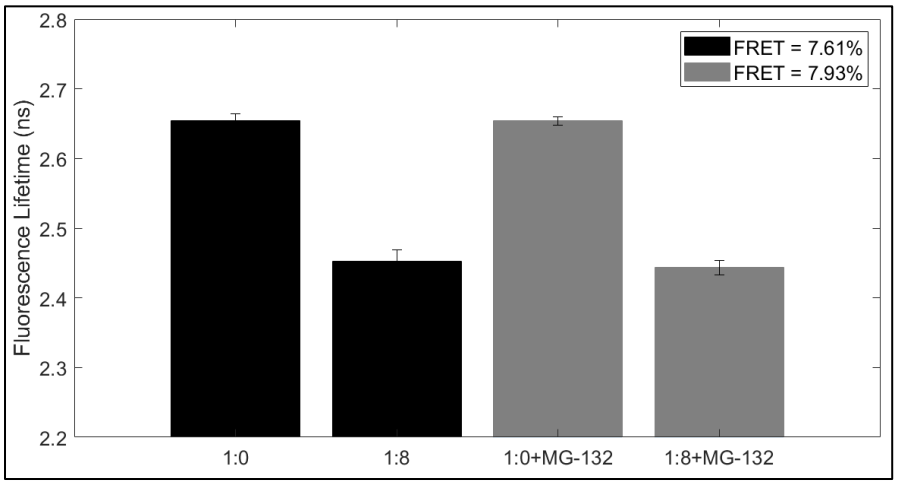

	1:0	1:8	1:0 MG-132	1:8 MG-132
1:0	-	9.59E-148	0.511	-
1:8	9.59E-148	-	-	7.37E-06
1:0 MG-132	0.511	-	-	1.14E-177
1:8 MG-132	-	7.37E-06	1.14E-177	-

Figure 2. Summary for FUS biosensor FRET experiment. Black: Untreated WT FUS biosensor FRET efficiency at 1:8 donor/acceptor. Gray: MG-132 treated WT FUS biosensor FRET efficiency. Table shows statistically significant (highlighted) p-values from two-sample t-tests assuming unequal variances.

High-Content Analysis of Stress Granules in FUS Expressing Neuronal Cell Line

In order to assess future hits obtained from drug screens, functional assays that test specific cellular functions need to be developed. FUS participates in many key cellular processes such as splicing, mRNA regulation and formation of stress and transport granules via LLPS. Moreover, recent research indicates that mutant FUS aggregates in the synapses of motor neurons, which may cause synaptic dysfunction [9]. We propose using high-content analysis as a means of validating functional hits that modulate FUS aggregation. Using fluorescence microscopy images, we developed a MATLAB script that extracts stress granule information. The code is capable of extracting stress granule cytoplasmic to nuclear ratio and area (see Appendix), which can be used as functional measures of proper FUS localization and kinetics, respectively. Ideally, future screens will be able to identify molecules that can rescue the mislocalization of FUS to the cytoplasm. In order to put the MATLAB script to test, we treated N2a cells with sorbitol (which causes FUS to mislocalize to the cytoplasm due to hyperosmotic stress) and MG-132 (a proteasome inhibitor that can trigger stress granule assembly). The resulting images are shown in Figure 3.

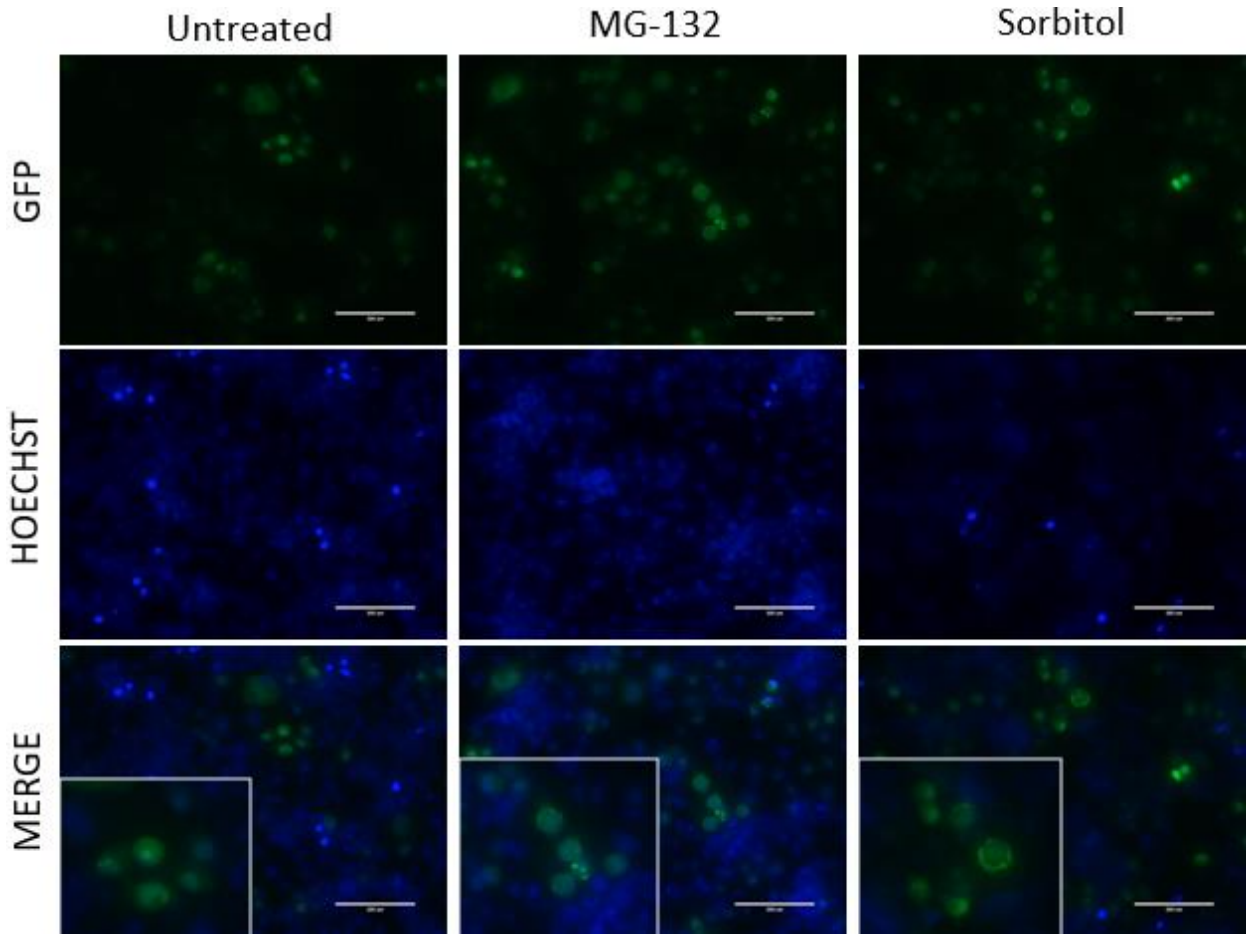

Figure 3. FUS-GFP expression in N2a cells upon stress granule inducing treatments (sorbitol and MG-132). Bottom row displays zoom in of merged GFP and Hoechst channels.

All conditions were quantified using the SG counting algorithm. In Figure 4, we display a sample segmentation of sorbitol treated cells, were a cytoplasmic FUS aggregate can be seen.

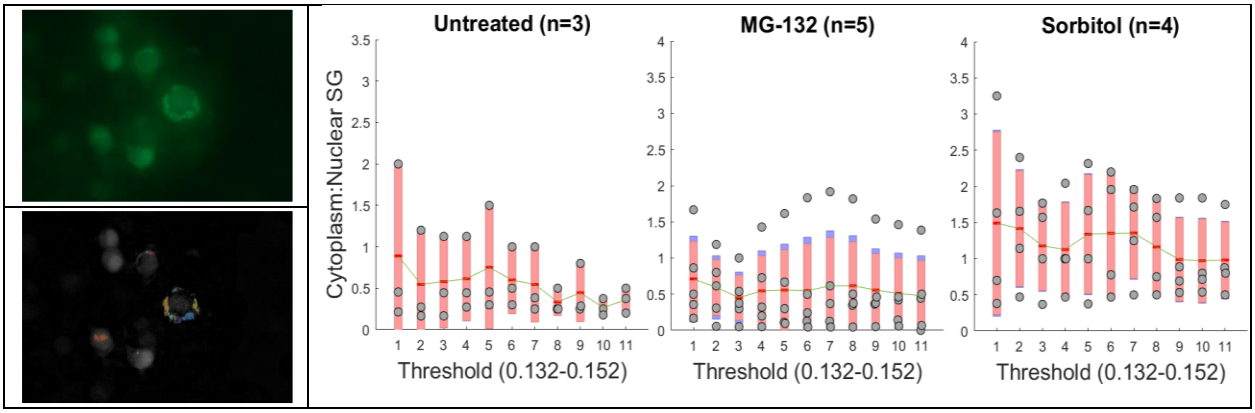

Figure 4. MATLAB Stress Granule Counter segmentation algorithm. Left: Sorbitol GFP and SG segmentation channels. Right: Sensitivity analysis of intensity threshold to cytoplasmic to nuclear ratio of FUS-GFP in untreated, sorbitol and MG-132 conditions. Each x axis tick represents an increase in intensity thresholding. Green line indicates mean cytoplasmic to nuclear ratio at each threshold. Value n indicates number of images used for each condition.

Automated Neurite Quantification in Model of Alpha-Synuclein Mutation

Alpha-synuclein has been implicated in several cellular processes related to axons and dendrites, as it has been associated with microtubule assembly [10]. For example, the aggregation of alpha-synuclein has been shown to decrease axonal transport, which is key for soma and nerve terminal maintenance [11]. Due to the significance of axons in the development of neurodegenerative diseases, we developed a neurite segmentation MATLAB script. We used neurospheres expressing WT αSyn and A53T αSyn, a mutant that recapitulates Parkinson's disease features in cultured neurons and mice. Figure 5 summarizes the results of the automated (Neurite) and manual (ImageJ) segmentation, which revealed a reduction in total neurite length per neurosphere arclength in the A53T αSyn condition when compared to wildtype. Specifically, the automated method reported a reduction of 41%, whereas the manual method reported a decrease of 49%.

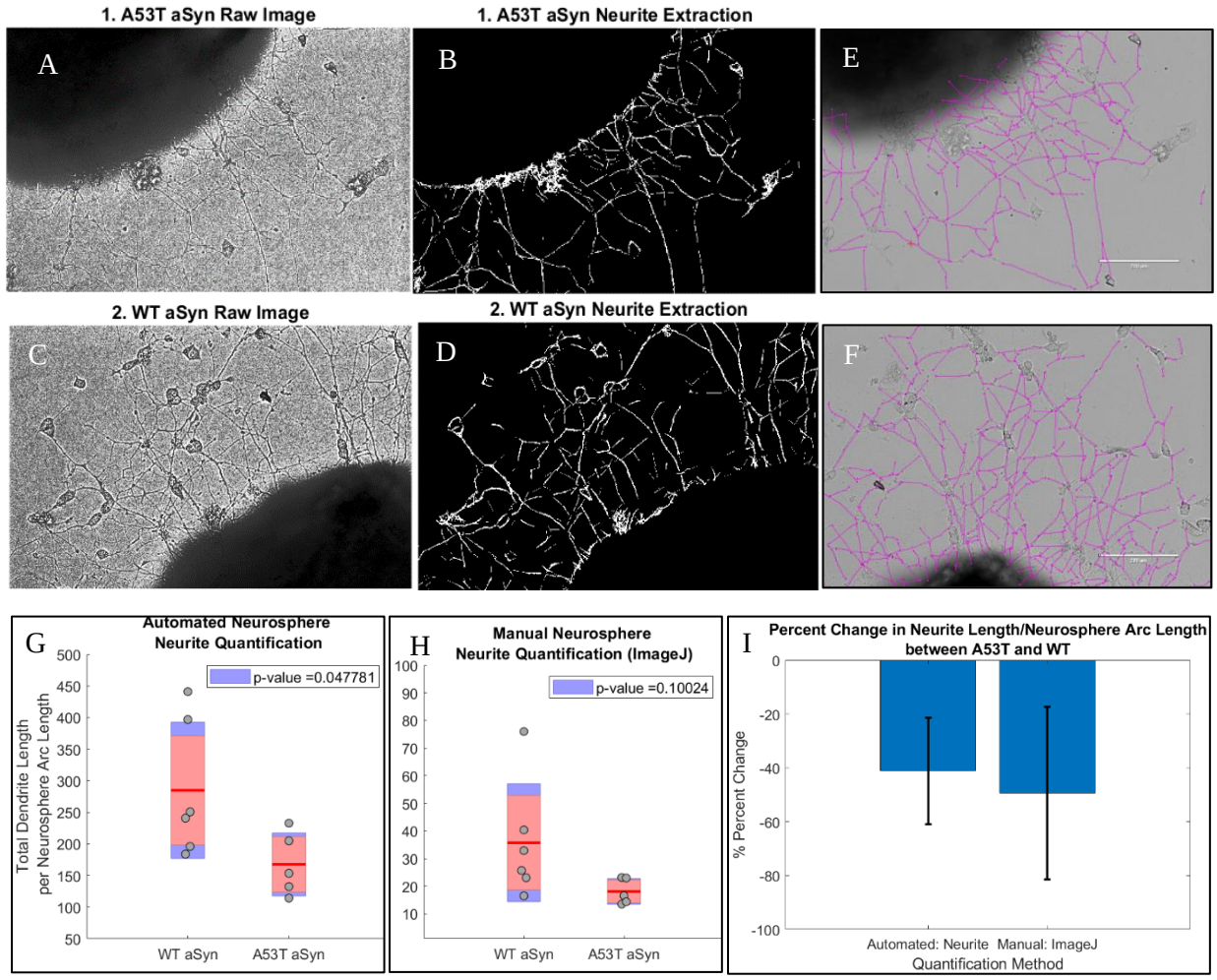

Figure 5. Segmentation of neurite outgrowth of WT αSyn (n = 6) and A53T αSyn (n = 5) expressing neurospheres. Sample images of automated segmentation using MATLAB Neurite algorithm (A-D). Manual segmentation (ImageJ) of A53T αSyn expressing neurosphere (E) and WT αSyn (F). Box plots of automated and manual neurite quantification normalized to neurosphere arclength (G-H). Comparison of neurite percent change of automated and manual quantification methods (I).

Discussion

There is a need for functional assays to validate hits obtained from FRET-based HTS drug discovery platforms. In this project, we have validated the viability of a FUS-FUS FRET-based biosensor for drug discovery in FUS-ALS and FUS-FTLD. Moreover, we implemented high-content image analysis scripts that can extract stress granule and neurite outgrowth information from fluorescent and brightfield microscopy.

Our previously engineered FUS FRET-based proved to be robust in terms of small variations in fluorescent lifetime of donor only and donor and acceptor expressing HEK-293 cells. This experiment provided a FRET cutoff (3 SD) for functional hits in future drug screens aimed at preventing FUS aggregation. Most importantly, the reduction in FRET required for a hit in this biosensor has been seen in other drug screens performed using the same platform [12]. Moreover, we found that blocking the proteasomal machinery via MG-132 was not sufficient to trigger FUS aggregation in HEK-293 cells.

On the other hand, in the neuronal N2a cell line, FUS did respond to both MG-132 and sorbitol treatment. One possible explanation to this is that in neuronal cell lines, FUS not only localizes to the nucleus but also to synapses [9]. In addition, it has been shown that FUS droplets form only above a certain FUS concentration (5 µM) and below a salt concentration of 100 mM [13,14]. It is possible that FUS was already localized to some extent in the cytoplasm of N2a cells, and the addition of MG-132 was sufficient to trigger its aggregation. On the other hand, the distribution of FUS in HEK-293 cells might be more restricted to the nucleus.

This hypothesis is supported by the results of the automated stress granule algorithm. Untreated cells were shown to have a cytoplasmic to nuclear ratio of FUS lower or equal to 1, which means FUS was distributed 50% in the nucleus and 50% in the cytoplasm, which correlates with fluorescence images. MG-132 treated cells showed similar nuclear to cytoplasmic ratios to untreated cells. However, images show bright FUS-GFP punctate, which might have formed from basal cytoplasmic FUS in addition to pathways activated due to MG-132, such as mitogenic signaling pathways [15]. Sorbitol treatment, which has been shown to cause FUS translocation to the cytoplasm via hypertonic stress [16], indeed caused higher cytoplasmic to nuclear ratios, as shown by imaging and segmentation. It is important to note that sorbitol-mediated FUS aggregation is largely independent from SG assembly pathways and active transport [16]. This might be the reason why sorbitol-induced FUS aggregates had visibly larger and irregular aggregates as compared to the smaller, spherical punctate caused by MG-132. The SG algorithm implemented had several limitations that need to be addressed before its utilization in actual functional assays. Careful analysis of segmented channels revealed that high intensity punctate were missed and larger structures were counted. This issue could be addressed by standardizing imaging and segmentation parameters.

The neurite extraction algorithm showed comparable results to manual extraction in terms of percent change in total neurites. Interestingly, we showed that A53T αSyn expressing neurospheres had lower total neurite per arclength unit than WT αSyn, as reported by other authors [17]. A53T mutants have been shown to be more aggregation-prone and cytotoxic than wildtype

alpha-synuclein [18]. The oligomerization of A53T is thought to destabilize microtubule cytoskeletal units, leading to neurite degeneration, a common feature of synucleinopathies [19]. The script developed was able to capture this process and it will serve useful in assessing rescue effects of αSyn-αSyn or αSyn-Tau FRET-based drug screen hits. Several factors contributed to error in the neurite segmentation code. Firstly, since extraction was performed via a single linear morphological structural element rotated by 360 degrees, the perimeter of cells were also segmented. In addition, thresholding and filtering of small objects might have deleted neurite networks. This most likely resulted in the difference in magnitude between the script and manual quantification. This issue needs to be addressed by exploring other segmentation strategies or improving the current one, as otherwise, the code will be limited to relative measurements to wildtype αSyn.

Conclusions & Future Directions

Regarding the FUS biosensor, future experiments will aim at improving the model for ALS pathology by screening both WT and disease causing FUS mutant. Preliminary mutagenesis was successful at creating GFP and RFP tagged FUS R495X, as well as FUS P525L (see Appendix for sequences and sample mutant expression). Comparing hits from WT FUS-FUS and mutant FUS-FUS will allow for drug screens aimed at disrupting toxic FUS aggregates.

In terms of the neurite segmentation algorithm, future iterations will aim at extracting more information such as number of neurite crossing (a measure of connectivity) and length per neurite. Moreover, it would be ideal to transition the culture strategy of neurospheres into microfluidic devices where neurite outgrowth is directed through channels. This strategy would minimize the error in the segmentation code and allow for a more robust assay to test other αSyn mutants and other proteins relevant to neurite growth processes.

In conclusion, this project was successful at validating our current FRET-based FUS biosensor and developing computational tools to quantify stress granules and neurite outgrowth. These tools will be utilized as high-content analysis assays to assess the rescue of WT phenotypes by drug screen hits.

References

1. Fuertes, Gustavo, Laura Nevola, and Santiago Esteban-Martín. "Perspectives on drug discovery strategies based on IDPs." *Intrinsically Disordered Proteins*. Academic Press, 2019. 275-327.
2. Uversky, Vladimir N. "Intrinsically disordered proteins and their (disordered) proteomes in neurodegenerative disorders." *Frontiers in aging neuroscience* 7 (2015): 18.
3. Birsa, N., Bentham, M.P., Fratta, P. "Cytoplasmic functions of TDP-43 and FUS and their role in ALS". Semin. Cell Dev. Biol. 2019.
4. Wolozin, B., Ivanov, P. "Stress granules and neurodegeneration". Nat Rev Neurosci 20, 649–666 (2019) doi:10.1038/s41583-019-0222-5
5. Bendor, Jacob T., Todd P. Logan, and Robert H. Edwards. "The function of α-synuclein." *Neuron* 79.6 (2013): 1044-1066.
6. Schaser, Allison J., et al. "Alpha-synuclein is a DNA binding protein that modulates DNA repair with implications for Lewy body disorders." *Scientific reports* 9.1 (2019): 1-19.
7. Hofweber, Mario, et al. "Phase separation of FUS is suppressed by its nuclear import receptor and arginine methylation." *Cell* 173.3 (2018): 706-719.
8. Lo, Chih Hung, et al. "An innovative high-throughput screening approach for discovery of small molecules that inhibit TNF receptors." *SLAS DISCOVERY: Advancing Life Sciences R&D* 22.8 (2017): 950-961.
9. Deshpande, Dhruva, et al. "Synaptic FUS localization during motoneuron development and its accumulation in human ALS synapses." *Frontiers in cellular neuroscience* 13 (2019): 256.
10. Carnwath, Tom, Raihan Mohammed, and Daniel Tsiang. "The direct and indirect effects of α-synuclein on microtubule stability in the pathogenesis of Parkinson's disease." *Neuropsychiatric disease and treatment* 14 (2018): 1685.
11. Volpicelli-Daley, Laura A. "Effects of α-synuclein on axonal transport." *Neurobiology of disease* 105 (2017): 321-327.
12. Lo, Chih Hung, et al. "Noncompetitive inhibitors of TNFR1 probe conformational activation states." *Science signaling* 12.592 (2019): eaav5637.
13. Wang, Jie, et al. "A molecular grammar governing the driving forces for phase separation of prion-like RNA binding proteins." *Cell* 174.3 (2018): 688-699.
14. Qamar, Seema, et al. "FUS phase separation is modulated by a molecular chaperone and methylation of arginine cation-π interactions." *Cell* 173.3 (2018): 720-734.
15. Wang, Hua-Qin, et al. "Inhibition of the JNK signalling pathway enhances proteasome inhibitor-induced apoptosis of kidney cancer cells by suppression of BAG3 expression." *British journal of pharmacology* 158.5 (2009): 1405-1412.
16. Hock, Eva-Maria, et al. "Hypertonic stress causes cytoplasmic translocation of neuronal, but not astrocytic, FUS due to impaired transportin function." *Cell reports* 24.4 (2018): 987-1000.
17. Liu, Guangwei, et al. "Alpha-synuclein promotes early neurite outgrowth in cultured primary neurons." *Journal of Neural Transmission* 120.9 (2013): 1331-1343.

18. Ostrerova-Golts, Natalie, et al. "The A53T α-synuclein mutation increases iron-dependent aggregation and toxicity." *Journal of Neuroscience* 20.16 (2000): 6048-6054.
19. Vekrellis, Kostas, et al. "Pathological roles of α-synuclein in neurological disorders." *The Lancet Neurology* 10.11 (2011): 1015-1025.

Appendix

A. SG area segmentation

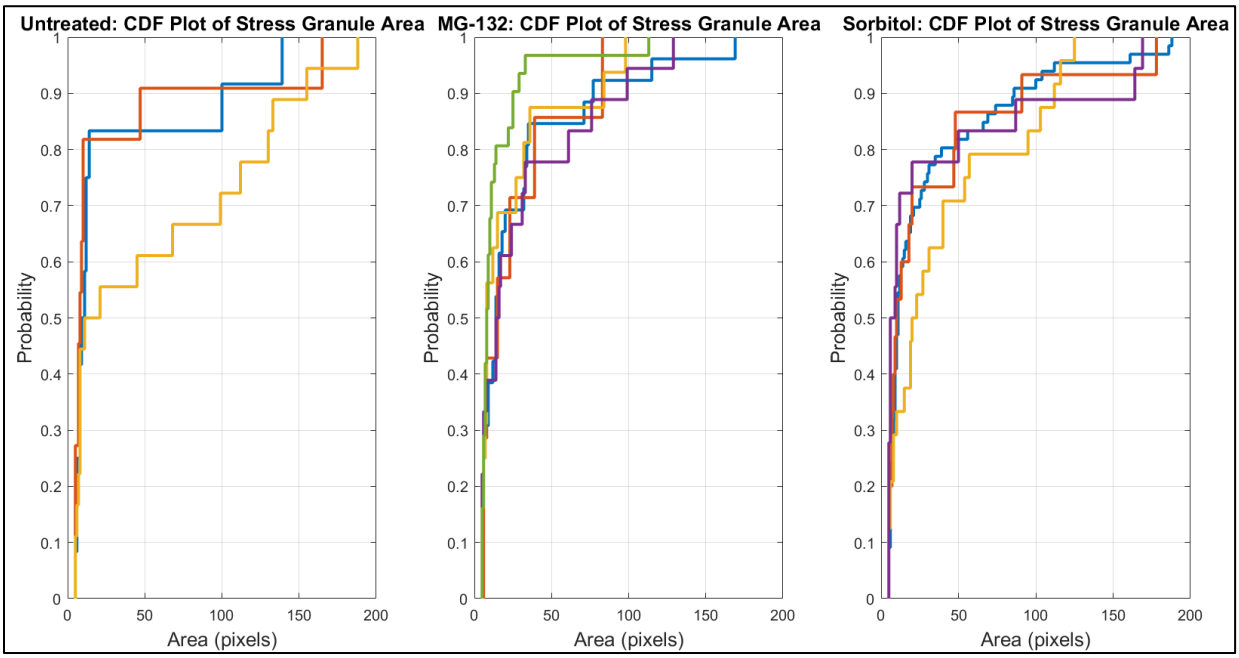

Figure 6. Cumulative distribution plots of stress granule area of FUS-GFP expressing N2a cells exposed to sorbitol and MG-132.

B. Preliminary mutant FUS results

Top row: WT FUS

Bottom row: mutant FUS

FUS+Linker – FUS-GFP R495X (1)

```
1398>taactacggggatgatcgtcgtggtggcagaggaggctatgatcgaggcggctaccggggccgcggcggggaccgtggaggcttccgagggggccggggt>1497
 166<taactacggggatgatcgtcgtggtggcagaggaggctatgatcgaggcggctaccggggccgcggcggggaccgtggaggcttc_______________<82

1498>ggtggggacagaggtggctttggccctggcaagatggattccaggggtgagcacagacaggatcgcagggagaggccgtatacgcgtgattacaaggatg>1597
  81<_____________________________________________________________________________acgcgtgattacaaggatg<63

1598>acgacgataagccaccggtcgccacc~~~~~~~~~~~~~~~~~~~~~~~~~~~~~~~~~~~~~~~~~~~~~~~~~~~~~~~~~~~~~~~~~~~~~~~~~~~~>1623
  62<acgacgataagccaccggtcgccaccatggtgagcaagggcgaggagcttcaccgggncccc<1
```

FUS+Linker – FUS-RFP R495X (1)

```
1399>aactacggggatgatcgtcgtggtggcagaggaggctatgatcgaggcggctaccggggccgcggcggggaccgtggaggcttccgagggggccggggtg>1498
```

```
  867>aactacggggatgatcgtcgtggtggcagaggaggctatgatcgaggcggctaccggggccgcggcggggaccgtggaggcttc________________>950

1499>gtggggacagaggtggctttggccctggcaagatggattccaggggtgagcacagacaggatcgcagggagaggccgtatacgcgtgattacaaggatga>1598
  951>________________________________________________________________________________acgcgtgattacaaggatga>970

1599>cgacgataagccaccggtcgccacc~~~~~~~~~~~~~~~~~~~~~~~~~~~~~~~~~~~~~~~>1623
  971>cgacgataagccaccggtcgccaccatggtgtctaagggcgaagagttgnccnggccccnctnn>1034
```

FUS+Linker – FUS-RFP P525L (3)

```
1500>tggggacagaggtggctttggccctggcaagatggattccaggggtgagcacagacaggatcgcagggagaggccgtatacgcgtgattacaaggatgac>1599
  853>tggggacagaggtggctttggccctggcaagatggattccaggggtgagcacagacaggatcgcagggagaggctgtatacgcgtgattacaaggatgac>952

1600>gacgataagccaccggtcgccacc~~~~~~~~~~~~~~~~~~~~~~~~~~~~~~~~~~~~~~~~>1623
  953>gacgataagccaccggtcgccaccatggtgtctaagggcgaagagctgactaagcccaccttt>1015
```

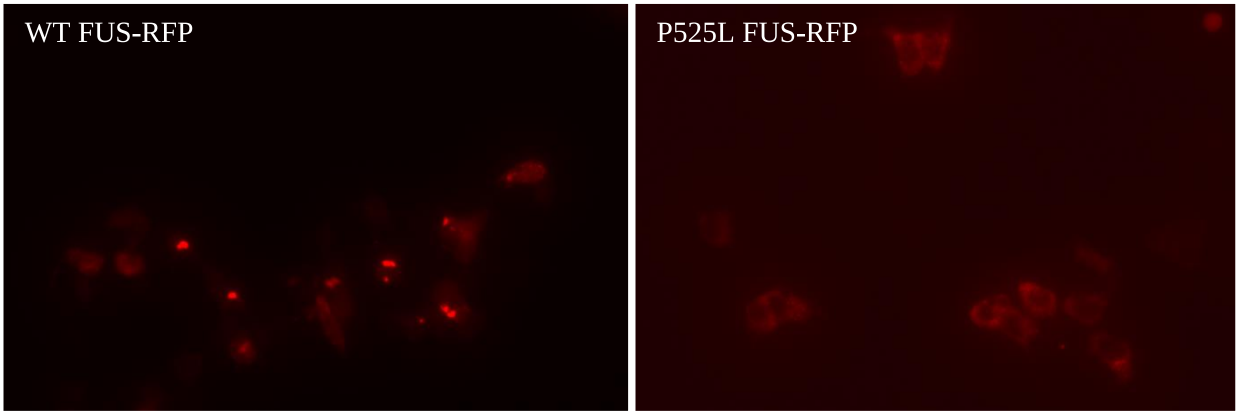

Figure 8. Results of QuickChange mutagenesis of FUS-GFP and FUS-RFP constructs. (Top) Alignment mutated FUS constructs to WT FUS. (Bottom) Expression of WT FUS-RFP and P525L FUS-RFP show distinct subcellular distribution of FUS. Remaining mutants had low mini-prep yields which resulted in low expression.